ACS EARTH AND SPACE CHEMISTRY

http://pubs.acs.org/journal/aesccq
Article

Effect of Acidity on Ice Nucleation by Inorganic–Organic Mixed Droplets

Ziying Lei,* Bo Chen, and Sarah D. Brooks*

Cite This: ACS Earth Space Chem. 2023, 7, 2562−2573
Read Online

ABSTRACT: Aerosol acidity significantly influences heterogeneous chemical reactions and human health. Additionally, acidity may play a role in cloud formation by modifying the ice nucleation properties of inorganic and organic aerosols. In this work, we combined our well-established ice nucleation technique with Raman microspectroscopy to study ice nucleation in representative inorganic and organic aerosols across a range of pH conditions (pH −0.1 to 5.5). Homogeneous nucleation was observed in systems containing ammonium sulfate, sulfuric acid, and sucrose. In contrast, droplets containing ammonium sulfate mixed with diethyl sebacate, poly(ethylene glycol) 400, and 1,2,6-hexanetriol were found to undergo liquid−liquid phase separation, exhibiting core−shell morphologies with observed initiation of heterogeneous freezing in the cores. Our experimental findings demonstrate that an increased acidity reduces the ice nucleation ability of droplets. Changes in the ratio of bisulfate to sulfate coincided with shifts in ice nucleation temperatures, suggesting that the presence of bisulfate may decrease the ice nucleation efficiency. We also report on how the morphology and viscosity impact ice nucleation properties. This study aims to enhance our fundamental understanding of acidity's effect on ice nucleation ability, providing context for the role of acidity in atmospheric ice cloud formation.

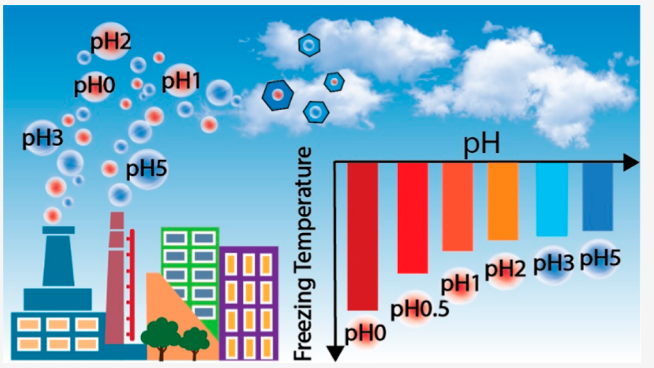

KEYWORDS: *aerosol acidity, ice nucleation, aerosol morphology, phase separation, viscosity*

INTRODUCTION

Atmospheric ice particles play a key role in determining the physical properties of clouds, thereby affecting the global radiative balance[1−6] and the hydrological cycle.[7] Additionally, ice particles can promote reactive heterogeneous chemistry, scavenge semivolatile gas species, and subsequently affect tropospheric composition.[8] Cirrus clouds are ubiquitous in the upper troposphere, covering 30% of the earth's area.[9] The abundance of cirrus clouds significantly impacts the earth's radiation budget, particularly considering that water vapor is the strongest greenhouse gas.[10,11] Furthermore, large radiative forcing uncertainties are associated with mixed-phase clouds containing both supercooled cloud droplets and ice particles.[12] In mixed-phase clouds, ice particles can significantly influence the supercooled liquid water content and determine the lifetimes of clouds.[13,14] Despite significant research advances in understanding atmospheric ice formation, a detailed understanding of the complex role of atmospheric aerosol particles in ice nucleation processes remains incomplete.

Determining the role of aerosols in ice nucleation is challenging because ice can form through multiple pathways. Homogeneous ice nucleation occurs spontaneously in pure water or aqueous solution droplets at temperatures below −38 °C and relative humidity well above the supersaturation with respect to ice (≥140% RH_{ice}).[15] However, at warmer temperatures and/or lower relative humidity, nucleation can occur through heterogeneous pathways, in which ice-nucleating particles (INPs) lower the nucleation barrier. Heterogeneous ice nucleation can occur through several different pathways, including immersion, deposition, or contact nucleation.[16,17] Although homogeneous ice nucleation has been considered to dominate cirrus cloud formation,[18−20] heterogeneous nucleation can increase cirrus occurrence and change the microphysical properties of cirrus clouds.[21,22]

Chemical composition strongly influences the conditions under which an INP can catalyze a freezing event. For example, mineral dust particles with large emission rates of up to 5000 Tg yr^{-1} are recognized as the most important INP type because of their generally effective ice nucleation ability.[23−26] Previous studies have found that dust particles activate as ice crystals at temperatures above −15 °C in the immersion

Received: August 24, 2023
Revised: November 8, 2023
Accepted: November 27, 2023
Published: December 11, 2023

https://doi.org/10.1021/acsearthspacechem.3c00242
ACS Earth Space Chem. 2023, 7, 2562−2573

mode.[23] Additionally, biological aerosols including bacteria, pollen, viruses, fungi, and phytoplankton can also act as effective INPs with freezing temperatures ranging from −3 °C for bacteria to below −38 °C for marine aerosols.[27−36] Furthermore, many studies have shown the pervasive presence of ammonium sulfate and sulfuric acid particles in the upper troposphere. These particles exhibit homogeneous freezing temperatures below −38 °C, playing a significant role in the formation of cirrus clouds.[37−41]

Organic aerosols often comprise a significant fraction of the ambient global tropospheric aerosol[42−46] and can contribute up to 90% by mass in tropical forested areas.[47,48] Secondary organic aerosol (SOA) is primarily formed through the oxidation of volatile organic compounds, resulting in lower vapor pressure products that either nucleate, condense, or undergo reactive uptake of existing particles. In addition to the variety in composition, organic aerosol may be present in the atmosphere in various phases, including solid, viscous liquid, or solution droplets, which complicates the determination of their contributions to ice crystal formation.

Previous research has shown that organic aerosols can promote heterogeneous ice nucleation via immersion, deposition, and contact freezing,[49−54] whereas other studies suggest that organic species tend to inhibit atmospheric ice formation.[55−57] Ice nucleation experiments have shown that naphthalene, methylglyoxal with methylamine, and isoprene-derived SOA particles are effective INPs.[58−60] However, the reported ice nucleation temperatures and mechanisms of α-pinene-derived SOA vary widely in the literature.[57,61−64] Differences in freezing temperature may result from variations in experimental processes, specifically residence times within the ice nucleation chambers, the selected conditions, and time scales of aerosol sample preprocessing prior to entering the respective chamber.[61,62,64] Ladino et al. investigated the ice nucleation ability of freshly generated α-pinene SOA from a flow tube with 2 min residence time as well as the α-pinene SOA generated from a smog chamber with 1.6 h residence time and precooling to mimic a cloud-processed particle. The result showed that the freshly generated α-pinene SOA froze at or even slightly above the homogeneous freezing line at temperatures between −40 and −60 °C while precooling the SOA particles to −40 °C dropped their ice nucleation onsets by up to 20% relative humidity with respect to ice.[61] Another study with highly viscous α-pinene SOA revealed freezing onsets below the homogeneous freezing threshold at temperatures between −39.0 and −37.2 °C.[62] Wagner et al. also investigated the ice nucleation ability of α-pinene SOA at temperatures from −68 to −20 °C and found that the unprocessed α-pinene SOAs were inefficient INPs at cirrus temperatures. However, the morphology and ice nucleation ability of the particles substantially changed, transforming from spherical to irregular, highly porous particles before and after the α-pinene SOA particles were activated to supercooled cloud droplets and underwent homogeneous freezing.[64] In a recent study, ice nucleation experiments conducted between −63 °C and −33 °C suggested that α-pinene SOA at different humidities (i.e., 40, 10, and <1% RH) can influence their ice nucleation.[63] This study shows that surrogates of boreal forest SOA particles promote only homogeneous ice formation in solution droplets.[63]

Extensive studies have investigated the heterogeneous ice nucleation efficiency of SOAs that exhibit a semisolid or glassy phase.[49,58,61,63,65] Interestingly, viscous organic liquids can serve as effective INPs through contact ice nucleation.[66] The diversity of phases that organic aerosols exhibit, such as solid, viscous liquid, or solution, further complicates the assessment of their role in ice nucleation processes. Increased viscosity in aerosols represents a barrier for immersion ice nucleation since the time required for water to diffuse within the particle and for a critical cluster of water molecules to arrange in an ice-like configuration may be substantially longer than in a solution.[67] Studies illustrate that the transition to a viscous or glassy phase can influence the mechanism that activates heterogeneous nucleation. For instance, Wang et al. studied the heterogeneous ice nucleation of naphthalene SOA particles and found that the particles had immersion freezing temperatures at −32.2 to −43.2 °C at ice saturation ratios = 1.48 to 1.35 and deposition freezing at −43.2 to −70.2 °C at ice saturation ratios = 1.52 to 1.36.[58] Their study indicated that particle phase state and viscosity influenced the particles' response to temperature and water uptake. In another previous study, Schill and Tolbert observed the immersion freezing temperature of the ammonium sulfate/1,2,6-hexanetriol mixtures at −33.2 to −53.2 °C at ice saturation ratios = 1.20 to 1.15 and no deposition freezing temperature until lower temperatures and higher ice saturation ratios = 1.31 to 1.2 were reached.[49] Notably, their study suggested that phase-separated mixtures could act as INPs regardless of whether the organic coating was liquid or glassy.[49] In the follow-up study, Schill et al. investigated the ice nucleation efficiency of aqueous SOA formed from the dark reactions of methylglyoxal with methylamine.[59] They discovered that the presence of ammonium sulfate decreased the viscosity of the aqueous SOA matrix, facilitating immersion ice nucleation at ice saturation ratios = 1.38 to 1.15 and temperatures ranging from −58.2 to −43.2 °C. The occurrence of ice nucleation, whether through homogeneous freezing of a viscous droplet or via heterogeneous pathways, is often dictated by the sample's specific conditions, including temperature and humidity, as well as the period before it enters the ice nucleation chamber.[63,64]

In addition to composition and phase, the acidity of particles has been shown to substantially impact SOA formation by modifying the reactive uptake rates of organic species through heterogeneous chemistry reactions.[68−70] For example, acid-catalyzed ring-opening reactions of epoxides that are taken up into particles have lifetimes on the order of seconds in acidic particles but on the order of days long in pH-neutral particles.[71] Atmospheric chamber experiments have observed that greater SOA formation occurs under acidic conditions (pH 1.5) compared to neutral conditions (pH 5).[70,72] Another study found that the ammonium sulfate seed particles with varying initial atmospheric acidity levels could lead to distinct differences in the morphology, phase state, and chemical composition of isoprene-derived SOA.[68] Other multiphase chemical processes where acidic pH conditions are important include water uptake,[73,74] hydrolysis,[75] metal ion dissolution,[76−78] and photolysis and OH reaction chemistry.[79,80] Recent studies have found that pH strongly affects liquid−liquid interactions, phase transitions, and ice nucleation ability of mineral dust particles.[81−84] With the increase in pH, the protonation state of organic acids changes, leading to the deprotonated organic acids having increased solubility in salt solutions due to increased ion−ion interactions. While the effects of particle acidity on these processes have been documented,[68,81,82,85,86] the effect of pH on the ice nucleation

https://doi.org/10.1021/acsearthspacechem.3c00242
ACS Earth Space Chem. 2023, 7, 2562−2573

Table 1. List of Inorganic and Organic Compounds Used in Ice Nucleation Measurements

compounds	formula	molecular weight (Da)	O/C	separation RH	refs
ammonium sulfate	$(NH_4)_2SO_4$	132.1	N/A	N/A	N/A
sucrose	$C_{12}H_{22}O_{11}$	342.3	0.92	N/A	You et al., 2015
diethyl sebacate	$C_{14}H_{26}O_4$	258.4	0.29	100.0 ± 6.2	You et al., 2013
poly(ethylene glycol)	$C_{2n}H_{4n}C_2O_{n+1}$	400.0	0.56	88.3 ± 6.6	You et al., 2013
1,2,6-hexanetriol	$C_6H_{14}O_3$	134.2	0.50	76.7 ± 6.2	You et al., 2013

ability of atmospheric relevant particles with different morphologies has yet to be explored. A more complete understanding of the critical factors (i.e., acidity and morphology) involved in ice nucleation is needed to better model cirrus formation in the upper troposphere and its effect on climate.

In the present work, we investigated the effect of acidity on homogeneous ice nucleation for particles composed of ammonium sulfate and their mixtures with sucrose. Additionally, we expanded our study to explore the heterogeneous ice nucleation behavior of particles undergoing liquid−liquid phase separation, specifically focusing on ammonium sulfate mixed with organic compounds such as diethyl sebacate, poly(ethylene glycol) 400, and 1,2,6-hexanetriol. For particles exhibiting a core−shell morphology, we observed that heterogeneous nucleation initiated within the core was accompanied by inclusion formation as the temperature decreased. Sulfuric acid was utilized across all experiments to adjust the pH levels, which ranged from −0.1 to 5.5. The ice nucleation experiments for isolated single droplets were performed by using a custom ice nucleation array inside a sealed cooling stage. Individual droplets were characterized by using Raman microspectroscopy, coupled with a temperature- and humidity-controlled cooling stage, to provide detailed information on droplet morphology and chemical composition throughout the ice nucleation process. Understanding the effect of the physicochemical properties of aerosols on ice nucleation is important for resolving the role of organic aerosols in ice cloud formation.

METHODS

Sample Preparation. Aqueous solutions were prepared using ultrapure water (UHPLC grade, Sigma-Aldrich) and the following chemicals: ammonium sulfate (Sigma-Aldrich), sulfuric acid (Millipore Sigma), sucrose (Sigma-Aldrich), diethyl sebacate, poly(ethylene glycol) 400, and 1,2,6-hexanetriol (TCI America). All chemicals were of >98.0% purity and used without further purification. No unexpected or unusually high safety hazards were encountered. The acidity of each solution was adjusted by the addition of 2 M sulfuric acid, resulting in pH values ranging from −0.1 to 5.5 ± 0.1, as measured using a pH probe (HI2002, HANNA Instrument). The homogeneously mixed solutions were prepared with concentrations of 0.3 M ammonium sulfate and 1 M sucrose. Detailed information on the concentrations is presented in Tables S1 and S2 of the supplementary document. Liquid−liquid phase-separated droplets were generated from a mixed solution of 0.3 M ammonium sulfate and 1% organic species at a 1:1 volume ratio of inorganic to organic components (Table 1). Each organic species was mixed separately with ammonium sulfate and sulfuric acid (AS/SA) to create droplets that exhibited phase separation at various pH levels. Diethyl sebacate, poly(ethylene glycol) 400, and 1,2,6-hexanetriol were selected because they are known to undergo liquid−liquid phase separation, while sucrose was chosen for comparison as a substance that does not undergo phase separation.

Ice Nucleation Experiments. A custom ice nucleation array was used to measure the freezing temperature of each sample, consisting of a cooling stage (LTS420, Linkam, Epsom Downs, UK), a ring LED light, a camera (EOS 5D Mark IV, Canon), and a computer system (Figure 1a). Liquid nitrogen

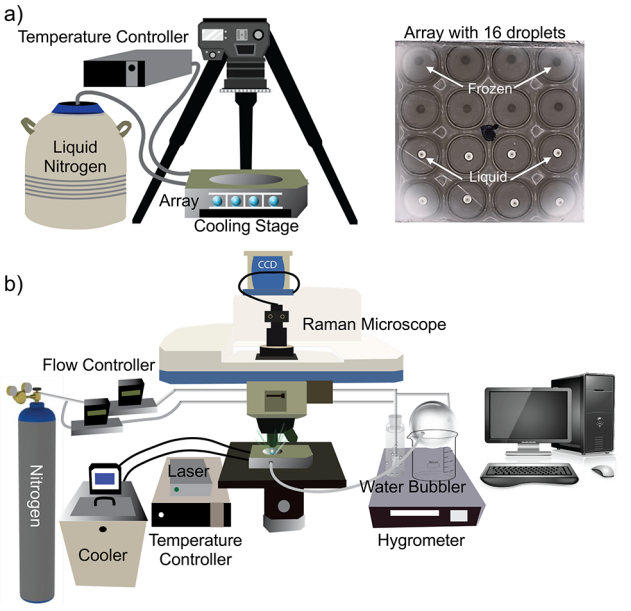

Figure 1. Experiment setup (a) ice nucleation setup using an array with 16 droplets; (b) Raman microspectroscopy setup to simultaneously measure ice nucleation of individual droplets, composition (Raman spectra), and phase separations (10× CCD images).

was used to cool the stage and control the temperature within 0.2 °C accuracy. Following our previously established procedure,[87] temperature calibration was performed in a range from −10 to −57 °C by measuring the melting points of droplets of dodecane (−9.6 °C), decane (−30.0 °C), and octane (−56.8 °C) in the sample state.[37,38] To further ensure the accuracy of our temperature measurements, freezing experiments with 2.0 μL of pure water droplets (UHPLC grade) were periodically conducted. These one-point checks yielded an average freezing temperature of −31.7 ± 0.6 °C standard deviation, which agrees with the freezing temperatures reported in the literature for similar-sized droplets of approximately 1−2 mm diameter.[88] This apparatus is based on our previous ice microscope apparatus,[87] with some modifications. The first modification was the addition of a polydimethylsiloxane spacer featuring 16 holes for testing the ice nucleation of 16 single droplets, isolated from one another and sealed with a glass coverslip. When one sample droplet freezes, the spacer ensures that the ice crystal will not scavenge

https://doi.org/10.1021/acsearthspacechem.3c00242
ACS Earth Space Chem. 2023, 7, 2562−2573

moisture from any remaining unfrozen droplets.[89] The spacer is fabricated from a 10:1 mixture of base polymer to curing agent (Sylgard 184, Dow Corning) poured onto a 3D printed mold that was custom-designed to represent the compartment array.[89] In our previous evaluation of viscous organic droplets as contact INPs, a viscous organic liquid droplet was placed adjacent to a droplet of pure water.[66] In contrast, each sample in this study is from an aqueous solution. Given the uniform distribution of solutes within the solution prior to freezing, it is assumed that the ice nucleation events observed are homogeneous. In the case of droplets from mixed inorganic−organic solutions that exhibit a core−shell morphology, the observed ice nucleation corresponds to heterogeneous freezing initiated at the core. The second modification was replacing optical microscopy with a high-resolution digital camera. While the images of sample droplets are not magnified, the high-resolution images allowed us to differentiate between liquid and frozen droplets. The camera also has the advantage of a wider viewing area, which allows for simultaneous viewing of all 16 sample compartments. The collected images are used to observe droplet freezing and determine the temperature of ice nucleation in postprocessing analysis. Furthermore, the images enable us to examine the morphology of the solution droplets to confirm different ice nucleation mechanisms in both liquid−liquid phase-separated and homogeneously mixed solution droplets.

In each experiment, 16 droplets were pipetted in the array, each undergoing 20 freezing events. This process was repeated three times, resulting in a total of 960 freezing events. At the start of each experiment, the 3D printed array with 16 holes was placed onto a hydrophobic glass slide (75 × 50 mm $L \times W$, Fisher Scientific), and a 2 μL droplet of the solution was pipetted in the center of each hole. A second hydrophobic glass slide was placed on top to isolate the individual samples and prevent the evaporation of droplets. The droplets were then cooled down from 10.0 to −50.0 °C at a cooling rate of 1.0 °C min^{-1}, and images of the droplets were recorded at every 0.1 °C. Next, the stage was warmed to 5.0 °C at a rate of 5 °C/min and held for 5 min to ensure that all the droplets had fully melted before the next cycle began.

Morphology and Chemical Characterization. Raman microspectroscopy was used to characterize the changes in phase-separated droplets and the chemical composition of the sample during freezing. A schematic of the experimental setup is shown in Figure 1b. The Raman system consists of an XploRA PLUS Raman spectrometer (Horiba Scientific) equipped with a 50 mW 532 nm Nd/YAG laser source and a CCD detector that is coupled to a confocal optical microscope (Olympus, 5×, 10×, and 50× objectives). A diffraction grating with 600 grooves/mm was used to obtain a spectral resolution of 1.7 cm^{-1}. Each Raman spectrum was collected over the range of 500−4000 cm^{-1} with acquisitions lasting 5 s each. The laser was set to 10% of its power capacity for molecular excitation to prevent the droplet from evaporating and heating up due to the laser.

To probe ice nucleation, the Raman system was outfitted with a Linkam LTS420 cooling stage, a hygrometer (EdgeTech DewPrime II, model 2000), and a Linkam temperature controller. In each experiment, a 2.0 μL single droplet was placed on hydrophobic quartz inside the cooling stage. A low humidified nitrogen flow was introduced into the sealed stage to prevent droplet evaporation throughout the experimental runs. The humidified flow was generated through the mixing of a flow of dry nitrogen (0.6 lpm) with another nitrogen flow that became saturated by passing through a glass bubbler (0.01 lpm). The hygrometer was used to monitor the dew point of the moist flow and ensure that condensation did not occur inside the cooling stage. The cooling stage was then sealed and cooled at 1.0 °C min^{-1} from 5.0 °C down to −40.0 °C. Microscopic images were automatically captured every 0.1 °C and Raman spectra were taken every 5.0 °C.

Viscosity Measurements. To address the role of viscosity in the ice nucleation of solution droplets, we conducted a series of experiments to measure the viscosity of aqueous AS/SA and AS/SA/diethyl sebacate as a function of pH (−0.1, 0.0, 1.0, 2.0, and 5.0) and temperature (23.0, 10.0, 5.0, 0.0, and −5.0 °C). A glass capillary viscometer (Ubbelohde Viscometer Cannon Instrument Co., size 1C) was filled with the solution and submerged into a cooling bath (Neslab ULT 80/95) held at a chosen temperature for 20 min to equilibrate before measurements were taken. The viscometry measurements were conducted ten times at each temperature setting, with the time scale for measuring the sample's movement through the viscometer ranging from 30 to 100 s.

Following our previously used viscometer measurements,[66] viscosity (n) was determined using the following equation

$$\eta = t \times c \times \rho \quad (1)$$

where η is viscosity, t is flow time (s), c is the viscometer constant, which was set to 0.03073 cSt/s for the Ubbelohde viscometer (model 1C) according to the manufacturer's calibration, and ρ is the density (g/mL) of the solution. The mass and volume of each solution with different pH values were measured to calculate the density. After each measurement, the glass capillary viscometer was thoroughly cleaned by soaking it in ethanol and rinsing it multiple times with UHPLC water. It was then fully dried by using nitrogen before the next measurement.

RESULTS AND DISCUSSION

To determine ice nucleation temperatures, droplet images were analyzed on a frame-by-frame basis using a custom-developed Python program from our laboratory. A nucleation event is identified by observing a distinct change in the opacity of the water droplet from a transparent liquid state to an opaque solid state between frames. In each experiment, four individual droplets with the same pH were placed in each row of the array, resulting in 16 droplets with four different pH levels. These droplets underwent 20 freezing cycles, and we repeated this entire process three times, culminating in a total of 960 independent freezing observations. t tests were conducted to compare the freezing temperatures of droplets at different pH values, with p-values < 0.05 being considered statistically significant.

The mean homogeneous freezing temperatures of AS/SA solution droplets across various pH levels are shown in Figure 2a. As a reference, the homogeneous freezing temperature of ammonium sulfate droplets without sulfuric acid (pH = 5.3) was observed at −26.8 ± 1.0 °C. Among the pH conditions tested, droplets with a pH of 3.8 exhibited the highest mean homogeneous freezing temperature at −25.9 ± 0.7 °C, while the most acidic droplets (pH = −0.1) displayed the lowest mean homogeneous freezing temperature at −37.4 ± 1.9 °C. These findings suggest an increasing trend in homogeneous freezing temperatures with decreasing acidity, indicating that greater acidity can depress homogeneous ice nucleation.

https://doi.org/10.1021/acsearthspacechem.3c00242
ACS Earth Space Chem. 2023, 7, 2562−2573

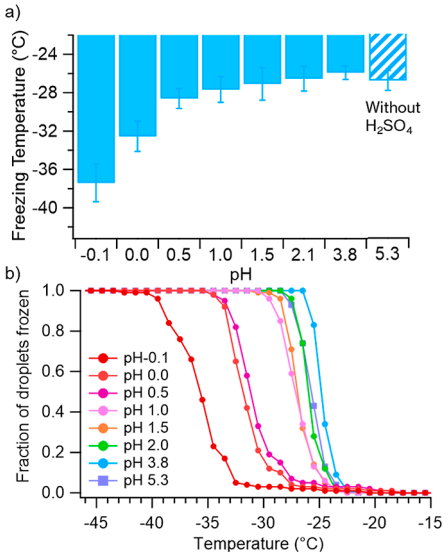

Figure 2. (a). Mean homogeneous freezing temperature of the AS/SA droplets. The error bars represent the standard deviation; (b) ice fraction of AS/SA droplets. Different colors represent different pH values.

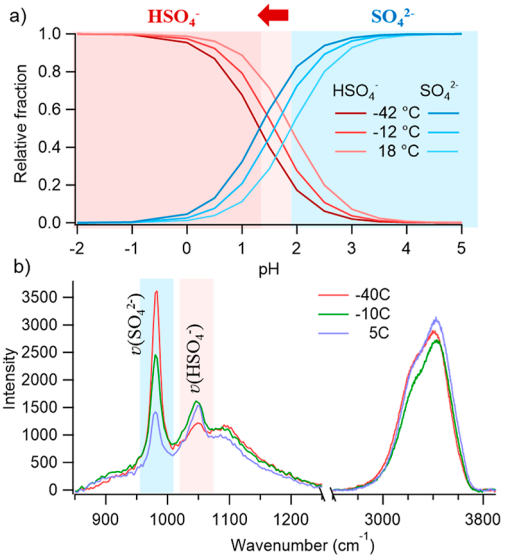

Figure 3. (a) Relative fraction for HSO_4^- and SO_4^{2-} concentrations as a function of pH and temperature, using the dissociation constant under different temperatures.[77] (b) Raman spectra of a pH = −0.6 sulfuric acid droplet under different temperatures.

Interestingly, no significant changes in homogeneous freezing temperatures were observed for droplets with pH values above 1. This suggests that a very high acidity level, pH < 1, is required to substantially influence the homogeneous freezing behavior of AS/SA droplets. The fraction of the droplets frozen as a function of temperature is shown in Figure 2b, revealing a correlation between decreasing homogeneous freezing temperatures and increasing acidity for droplets with pH values below 1.

To further explore the characteristics of the solution above and below pH 1, we first consider the simplified case of sulfuric acid in water. Sulfuric acid dissociates through a two-step process

$$H_2SO_4 \rightarrow H^+ + HSO_4^- \quad (2)$$

$$HSO_4^- \rightarrow H^+ + SO_4^{2-} \quad (3)$$

In a previous study, Knopf et al. investigated the dissociation of sulfuric acid solutions as a function of concentration and observed that the degree of dissociation of HSO_4^- increases with decreasing temperature.[90] The relative fraction of the HSO_4^- and SO_4^{2-} ions under different temperature conditions is calculated and the results are presented in Figure 3a. At pH < 1, bisulfate (HSO_4^-) dominates, comprising approximately 90% of the ions, while at pH > 4, sulfate (SO_4^{2-}) dominates, accounting for approximately 99% of the ions at room temperature. It has been observed that as the temperature decreases from 18 to −42 °C, the equilibrium between sulfate and bisulfate ions shifts toward a lower pH of 1.4 from an initial pH of 1.9. This shift in equilibrium suggests that lower temperatures enhance the dissociation of HSO_4^- ions, leading to an increase in the relative fraction of bisulfate ions.

Next, Raman spectra were collected on a sulfuric acid droplet with pH = −0.6 to confirm the changes in composition with temperature. The spectra showed vibration bands $\nu(SO_4^{2-})$ at 980 cm^{-1} and $\nu(HSO_4^-)$ at 1040 cm^{-1} (Figure 3b).[91,92] The intensity of the sulfate peak increased as the temperature decreased, consistent with the previous findings. This shift in the $\nu(HSO_4^-)$ to $\nu(SO_4^{2-})$ ratio coincided with significant differences in homogeneous freezing temperatures observed for AS/SA droplets with pH values ≤ 1. These results suggest that higher relative fractions of HSO_4^- ions within the droplets may potentially drive their ice nucleation ability. We hypothesize that the ratio of HSO_4^- to SO_4^{2-} may play a crucial role in determining the ice nucleation properties of inorganic−organic droplets as well.

To assess the impact of acidity on the ice nucleation in homogeneously mixed inorganic−organic droplets, the mean homogeneous freezing temperature of AS/SA/sucrose at various pH values is shown in Figure 4a. The results indicated a trend in homogeneous freezing temperature similar to that observed for AS/SA, with the lowest mean homogeneous freezing temperature of −36.9 ± 2.8 °C for droplets at pH −0.1 and the highest of −21.8 ± 0.9 °C for droplets at pH 5.3. Unlike AS/SA droplets, the ice fraction of AS/SA/sucrose droplets exhibited distinct variations across different pH levels, except at pH 1.5 and 2.0, where no significant difference was observed (Figure 4b).

Raman spectra of AS/SA/sucrose droplets with pH values of 0.0, 1.0, and 5.3 are shown in Figure 4c. A strong sulfate peak $\nu_s(SO_4^{2-})$ at 973 cm^{-1} and the bisulfate $\nu_s(HSO_4^-)$ peak at 1041 cm^{-1} are clearly discernible in the Raman spectra for droplets at all three pH values.[93−96] As seen in the AS/SA system, the ratio of the sulfate to bisulfate peaks shifts with the acidity of the droplet. For example, a larger bisulfate peak was observed for droplets at pH 0.0 compared to those at pH 5.3. Peaks indicative of organic activity were observed in all droplets. Specifically, peaks at 1060 and 1129 cm^{-1} are assigned to ν(C−O) and δ(COH), respectively.[97,98] The asymmetric carbon−hydrogen bend, δ(C−H), of methylene at 1456 cm^{-1},[99,100] carbonyl ν(C═O) at 1650 cm^{-1}, and symmetric and antisymmetric of methyl and methylene stretches were observed in the ν(C−H) region between 2800 and 3000 cm^{-1}.[94,101] The peak at 3230 cm^{-1} is assigned to ammonium $\nu(NH_4^+)$[102] and the hydroxyl ν(O−H) peak

https://doi.org/10.1021/acsearthspacechem.3c00242
ACS Earth Space Chem. 2023, 7, 2562−2573

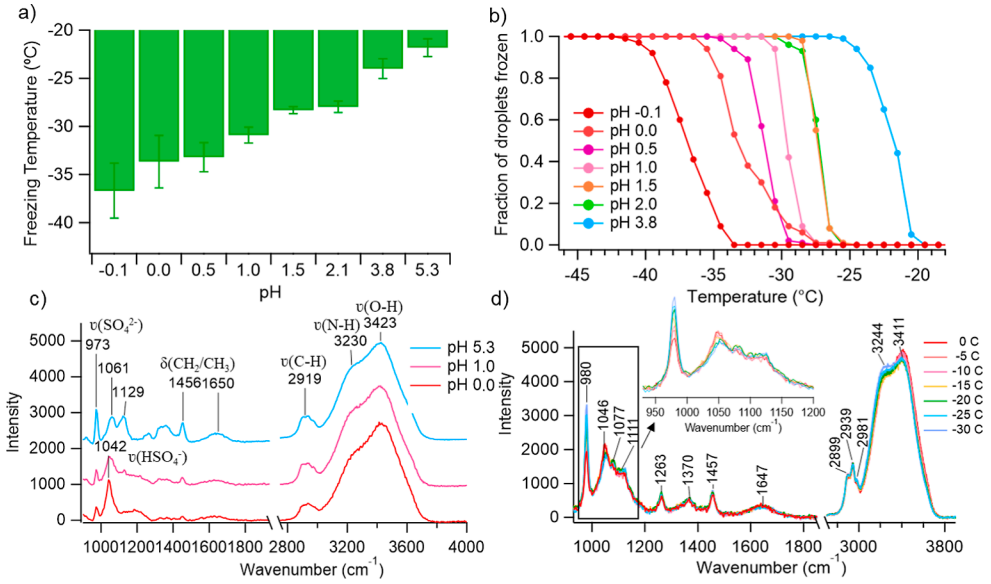

Figure 4. (a) Mean homogeneous freezing temperature of the AS/SA/sucrose system (1:1 ammonium to sucrose ratio) with varying pH values, the error bars represent one standard deviation; (b) ice fraction of AS/SA/sucrose; (c) Raman spectra of AS/SA/sucrose with pH 0.0, 1.0, and 5.3; (d) Raman spectra of pH = 0.0 AS/SA/sucrose under different temperatures.

was observed at 3423 cm^{-1} from either the sucrose or water from the aqueous droplet.[94,103]

Raman spectra of the inorganic−organic droplets were taken at different locations within the single droplet (Figure 4c). The AS/SA/sucrose droplets did not exhibit core−shell morphology at varying pH levels from microscopic images, and the spectra were taken both at the edge and center of the droplet present consistent composition. This suggests that the AS/SA/sucrose droplets were uniformly mixed across all pH values (−0.1 to 5.3), which is consistent with findings from previous studies.[104,105] Additionally, the chemical composition of the droplets was characterized under different temperature conditions. Specifically, at pH 0, the Raman spectra (Figure 4d) revealed a shifting ratio of sulfate to bisulfate peaks as a function of temperature, suggesting an increase in sulfate concentrations within the droplet at lower temperatures. This result provides further indication that higher concentrations of bisulfate ions may enhance the ice nucleation ability of these homogeneous mixed inorganic−organic droplets.

Previous studies have shown that the freezing temperatures of ammonium sulfate, sulfuric acid, and other organic compounds can be predicted by changes in water activity.[37,39,40,106] To evaluate whether the observed trends in freezing temperatures of homogeneous droplets could be predicted with water activity, we utilized the Extended Aerosol Inorganics Model (E-AIM) to estimate water activity in homogeneously mixed inorganic and organic systems.[107] Detailed concentrations and corresponding calculated water activities for AS/SA and AS/SA/sucrose at various pH levels are shown in Tables S1 and S2. For the AS/SA system, the results indicated that the water activity increases with a decrease in acidity, ranging from 0.94 at pH −0.1 to 0.98 at pH 0.5 solution. However, the water activity levels off between approximately 0.98 and 0.99 for pH values ranging from 1.5 to 5. In comparison, the freezing temperatures increased more steadily with decreased acidity, from approximately −37.4 °C at pH −0.1 to −26.8 °C at pH 5.3.

Similarly, for the AS/SA/sucrose system, the trend in water activity was not found to align closely with the observed changes in freezing temperature. It was also noted that the E-AIM model analysis might not accommodate the more complex cases of phase-separated particles. Our findings suggest that while increased water activity may promote warmer freezing temperatures as reported in previous studies,[106] the observed changes in freezing temperatures were more closely aligned with shifts in composition as indicated in the Raman spectra.

The role of acidity on ice nucleation may differ for phase-separated droplets that exhibit a core−shell morphology. To investigate this, AS/SA solutions were mixed with different organic compounds, including diethyl sebacate, poly(ethylene glycol) 400, and 1,2,6-hexanetriol; each of these mixtures has been observed to undergo liquid−liquid phase separation at high relative humidity (RH > 76.7%).[105] In our study, inorganic−organic mixed droplets with different pH values consistently exhibited liquid−liquid phase separation with a core−shell morphology. These findings align with previous work by Bertram et al., who reported that binary mixtures of organic species and sulfates typically undergo phase separation if the O/C ratio of the organic component is below 0.7.[108] Furthermore, the phase separation of the mixtures in this study showed no dependence on pH or temperature, which is consistent with previous studies.[49,109]

To ensure that the ammonium sulfate droplets were fully coated at room temperature and relative humidity (~50%), the microscopic images were collected under different temperatures at 10× magnification of a single droplet (Figure 5a). The core−shell structure was further confirmed using Raman spectra, which provided detailed chemical compositions of the droplet core and shell (Figure 5b). The Raman spectra showed peaks presenting $\nu_s(SO_4^{2-})$ at 972 cm^{-1}, $\nu_s(HSO_4^-)$ at 1042 cm^{-1}, and the broad ν(N−H) region around 3418 cm^{-1} indicating sulfate, bisulfate, and ammonium located primarily in the particle core.[93−96,110−112] Additionally, a peak at 1438 cm^{-1} was assigned to the methyl/methylene group bend $\delta(CH_3/CH_2)$, while a carbonyl group ν(C═O) mode was observed at 1725 cm^{-1},[113] indicating the presence of diethyl sebacate in the shell. Peaks between 2800 and 3000 cm^{-1},

https://doi.org/10.1021/acsearthspacechem.3c00242
ACS Earth Space Chem. 2023, 7, 2562−2573

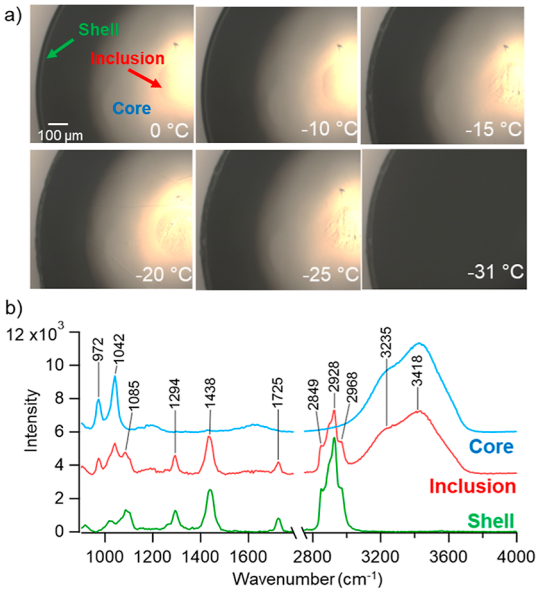

Figure 5. (a) Microscopic images of a single AS/SA/diethyl sebacate droplet with pH 0 under different temperature conditions; (b) Raman spectra of the droplet collected at different locations of the droplet.

indicative of the C−H stretching region, were observed in the Raman spectra of standard diethyl sebacate in Figure S5.

To determine whether the morphology of the phase-separated droplet changes during freezing, we captured microscopic images at different temperatures. In Figure 5a, as temperatures gradually decreased to −5 °C, a droplet consisting of AS/SA/diethyl sebacate at pH 0 displayed a core−shell morphology with an inclusion. The Raman spectrum of the inclusion was collected at −5 °C, suggesting that the inclusion contained both organic compounds from the AS/SA/diethyl sebacate mixture, as evidenced by the ν(C=O) at 1085 cm^{-1} within the inclusion. Further cooling to −15 °C resulted in the organic shell losing its smooth surface, indicative of a transition from a liquid to a semisolid/solid state. Notably, the absence of the hydroxyl ν(O−H) peak at 3428 cm^{-1} in the shell implies that the coating of the droplet likely became solid or glassy. As the temperatures dropped below −20 °C, the morphology of the inclusion changed from a round to an irregular shape, indicating that the liquid phase shifted to a more solid state. It is interesting to note that the AS/SA/diethyl sebacate droplet froze when the core froze at −31 °C, as shown in the last microscopic image in Figure 5a. Despite the phase changes in the shell and inclusion being observed at different temperatures, the initiation of heterogeneous freezing was noted at the core of a phase-separated droplet rather than at the shell. This result is supported by our Raman spectra, which show the absence of water in the shell at −5 °C, suggesting that the organic shell lacks the capability to actively promote or initiate a freezing event. In terms of ice nucleation, a prior study by Wise et al. suggested that organic-sulfate particles with incomplete organic coatings can effectively initiate ice nucleation, and even uncoated ammonium sulfate could catalyze new ice formation,[114] findings which are in agreement with those of this study.

In Figure 6, the heterogeneous core freezing temperatures were measured for the droplets composed of AS/SA mixed with each of the organic compounds including diethyl sebacate, poly(ethylene glycol) 400, and 1,2,6-hexanetriol across a range of pH values from −0.1 to 5.5. Although there is no significant difference in freezing temperatures for the mixture droplets with pH > 1.0, the ice fraction for each organic mixture displays different trends (Figure 6a−c). Specifically, there was a noticeable increase in the heterogeneous core freezing temperatures as pH increased from −0.1 to 0.5, which then stabilized at similar temperatures for pH > 1.0. It is worth noting that the AS/SA/poly(ethylene glycol) samples showed a trend of decreasing heterogeneous core freezing temperature with increasing acidity for droplets with pH < 1.5. In contrast, the AS/SA/diethyl sebacate mixture

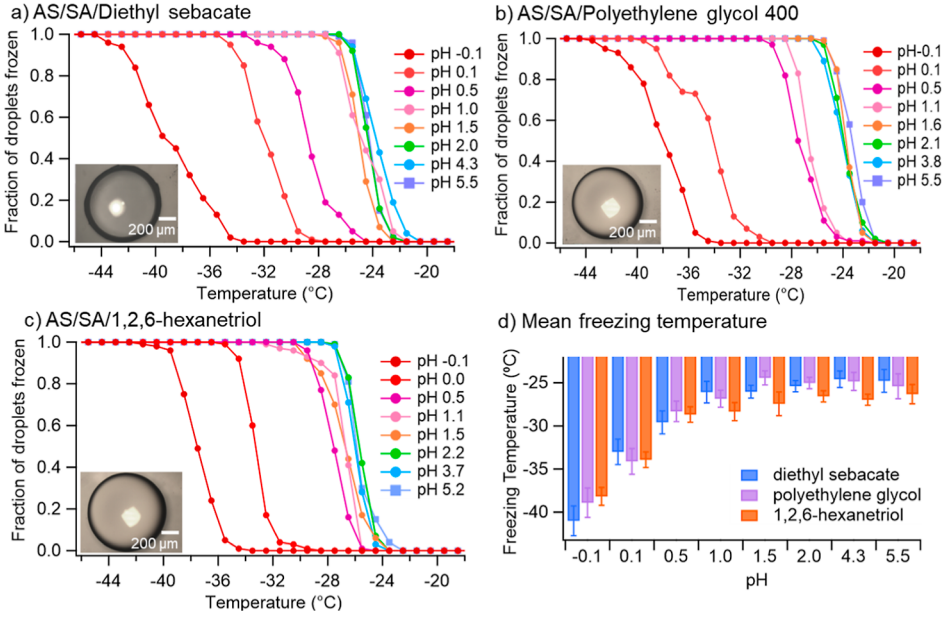

Figure 6. Ice fraction of phase-separated droplets with ~100 freezing cycles: (a) ice fraction of AS/SA mixed with diethyl sebacate; (b) ammonium sulfate mixed with poly(ethylene glycol) 400; (c) AS/SA mixed with 1,2,6-hexanetriol; the error bars represent standard deviation; (d) mean heterogeneous core freezing temperature of four different mixture systems with varying pH values.

https://doi.org/10.1021/acsearthspacechem.3c00242
ACS Earth Space Chem. 2023, 7, 2562−2573

samples showed a similar trend for droplets with pH < 1.0, and the AS/SA/1,2,6-hexanetriol mixture samples exhibited this trend for droplets with pH < 0.5.

The mean heterogeneous core freezing temperatures of different organic mixtures with varying acidities can be seen in Figure 6d. Our results suggest that droplets with a lower pH exhibit poor heterogeneous ice nucleation efficiency compared to those with higher pH levels. Specifically, the lowest heterogeneous core freezing temperatures were observed for the mixtures of AS/SA/diethyl sebacate (−41.0 ± 1.7 °C), AS/SA/poly(ethylene glycol) 400 (−38.9 ± 1.7 °C), and AS/SA/1,2,6-hexanetriol (−38.2 ± 1.0 °C), respectively. Overall, our findings indicate that these phase-separated droplets serve as more effective ice nuclei as their acidity decreases.

The differences in nucleation temperatures observed for each organic-sulfate mixture may be attributed to the varying phase states (i.e., semisolid or glassy) of the respective organics and the inclusion formation. To elucidate why these phase-separated droplets become more efficient ice nuclei under less acidic conditions, we collected Raman spectra of an AS/SA/diethyl sebacate mixture with different pH levels at different temperatures (Figures S1−S4). The Raman spectra showed a strong sulfate $\nu_s(SO_4^{2-})$ peak at 973 cm^{-1} and the bisulfate $\nu_s(HSO_4^-)$ peak at 1041 cm^{-1} in the core of the droplets with pH from 0.0 to 1.0 under room temperature. As the temperature decreased, a higher concentration of sulfate was observed within the core of the droplets, while no sulfate peak was detected in the shell. This result is consistent with our previous findings for the AS/SA/sucrose mixture. Despite the presence of full organic coatings, these mixed organic-sulfate droplets were found to exhibit ice nucleation efficiency comparable to that of the freezing temperature of inorganic AS/SA (with homogeneous freezing temperatures ranging from 37.4 to 26.8 °C for pH values ranging from −0.1 to 5.3). The organic coating of these liquid−liquid phase-separated droplets did not significantly facilitate ice nucleation across varying pH conditions.

A previous study observed water vapor diffusing through the liquid coating to facilitate ice nucleation on the ammonium sulfate cores.[49] Particles that have undergone liquid−liquid phase separation, composed of inorganic and organic materials, appear to nucleate ice with an efficiency nearly on par with that of pure ammonium sulfate when in the depositional mode.[49] When the organic coating becomes semisolid or glassy, it may hinder the diffusion of water vapor, leading to depositional ice nucleation on the organic shell. However, in our study, the freezing cycles were conducted without introducing additional water vapor, which led to no observed water uptake or diffusion through the shell from outside the particle. While the initiation of heterogeneous ice nucleation by the core of the droplet was observed, it is possible that the freezing of the core was aided by the interface with the shell, which was noted to visibly roughen at its edges as the temperature decreased, or by the presence of inclusions within the core. Future work will focus on conducting detailed and quantitative characterizations of morphological changes of core−shell systems under various temperatures and coating thicknesses to gain further insights into the influence of these changes on the heterogeneous ice nucleation ability of droplets with varying pH values.

In addition to morphology, previous studies have shown that the viscosity of organic compounds increases as temperature decreases from 20 to −40 °C,[66] which can impede heterogeneous ice nucleation due to retarded water diffusion. Therefore, we measured the viscosity of AS/SA and AS/SA/diethyl sebacate systems across various pH values ranging from −0.1 to 5.0 under different temperatures (Figure 7a,b). The

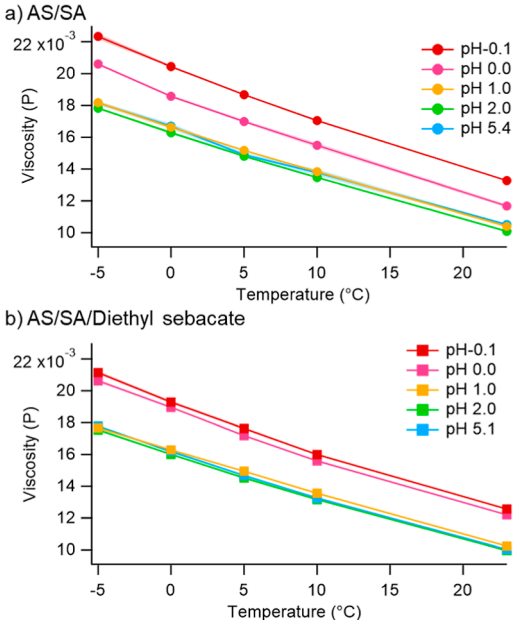

Figure 7. Viscosity of (a) AS/SA mixture; (b) AS/SA/diethyl sebacate mixture under different temperatures. Different colors represent different pH values.

viscosity as a function of the temperature and acidity was observed for both mixture systems. At room temperature, slight differences in viscosity were observed across the AS/SA system with varying pH. For example, the viscosity at pH −0.1 was 0.013 Pa·s compared to 0.010 Pa·s at pH 5.0. However, the more acidic AS/SA solutions (pH = −0.1 and 0.0) are more viscous than less acidic solutions (pH 1.0, 2.0, and 5.0). Additionally, the decrease in temperature causes a dramatic increase in viscosity of more than 2 orders of magnitude for AS/SA. At −5 °C, the viscosities were recorded at 0.022 Pa·s for pH −0.1 and 0.018 Pa·s for pH 5.0. A similar trend was found in the AS/SA/diethyl sebacate mixture, with increasing acidity and decreasing temperatures resulting in higher viscosities. It is interesting to note that the viscosity trend across different pH levels paralleled those of freezing temperatures; a higher acidity was associated with increased viscosity and lower freezing temperatures. This suggests that acidity may play a role in altering the viscosity of droplets, potentially modifying their ice nucleation properties.

CONCLUSIONS

To the best of our knowledge, this is the first study to explore the impact of pH on ice nucleation abilities in a range of inorganic (AS/SA) and inorganic-organic mixed aerosols (AS/SA/sucrose, AS/SA/diethyl sebacate, AS/SA/poly(ethylene glycol) 400, and AS/SA/1,2,6-hexanetriol), across pH conditions from −0.1 to 5.5. The mean homogeneous freezing temperatures of AS/SA droplets fall between −37.4 and −25.9 °C for pH values from −0.1 to 3.8. In general, the observed changes in ice nucleation parallel and may be driven by changes in water activity.[106] The mean homogeneous freezing temperature of droplets containing 3.8% weight percent ammonium sulfate without sulfuric acid and with a pH of

https://doi.org/10.1021/acsearthspacechem.3c00242
ACS Earth Space Chem. 2023, 7, 2562−2573

5.3 was measured to be −26.8 °C. This value is notably higher than the freezing temperature observed in a previous study, where 6% weight percent ammonium sulfate droplets were reported to freeze at −41 °C.[38] This discrepancy may be attributed to the different relative concentrations of ammonium sulfate and water in the respective studies, as well as differences in droplet sizes.

We also measured the mean heterogeneous core freezing temperatures of various inorganic−organic mixtures [AS/SA/diethyl sebacate, AS/SA/poly(ethylene glycol) 400, and AS/SA/1,2,6-hexanetriol] over a range of pH values spanning from −0.1 to 5.5. The observed heterogeneous core freezing temperature ranges for these mixtures were as follows: −41.0 to −24.8 °C for AS/SA/diethyl sebacate, −38.9 to −25.4 °C for AS/SA/poly(ethylene glycol) 400, and −38.2 to −26.3 °C for AS/SA/1,2,6-hexanetriol.

Understanding the detailed physicochemical properties of aerosol particles is crucial for gaining insights into atmospheric ice cloud formation. Our results indicate that freezing temperatures are strongly influenced by aerosol acidity, with increased acidity resulting in lower freezing temperatures. This correlation is primarily attributed to the presence of sulfate and bisulfate fractions in the droplets, which increase as the temperature decreases. We also show that the viscosity of the inorganic−organic mixture increases under more acidic conditions and at lower temperatures, suggesting that viscosity may contribute to the reduced ice nucleation ability due to retarded water diffusion. This inorganic−organic particle behavior highlights the importance of detailed physicochemical characterization considering their crucial role in cloud condensation nuclei, INP activity, and ice cloud formation.

■ ASSOCIATED CONTENT

Supporting Information

The Supporting Information is available free of charge at https://pubs.acs.org/doi/10.1021/acsearthspacechem.3c00242.

Detailed concentration information on ammonium sulfate mixed with sulfuric acid; detailed concentration information on ammonium sulfate mixed with sulfuric acid and sucrose; Raman spectra of pH 0 ammonium sulfate mixed with diethyl sebacate; Raman spectra of pH 0.5 ammonium sulfate mixed with diethyl sebacate; Raman spectra of pH 1 ammonium sulfate mixed with diethyl sebacate; Raman spectra of pH 1.5 ammonium sulfate mixed with diethyl sebacate; and Raman spectra of diethyl sebacate (PDF)

■ AUTHOR INFORMATION

Corresponding Authors

Ziying Lei − *Department of Atmospheric Science, Texas A&M University, College Station, Texas 77843, United States;* orcid.org/0000-0003-3071-0698; Email: lziying@tamu.edu

Sarah D. Brooks − *Department of Atmospheric Science, Texas A&M University, College Station, Texas 77843, United States;* orcid.org/0000-0001-8185-9332; Email: sbrooks@tamu.edu

Author

Bo Chen − *Department of Atmospheric Science, Texas A&M University, College Station, Texas 77843, United States*

Complete contact information is available at: https://pubs.acs.org/10.1021/acsearthspacechem.3c00242

Funding

This work was supported by the National Science Foundation under Grant ECS Award 1808256. Z.L. acknowledges support from the Texas A&M Geoscience Future Faculty Postdoctoral Fellowship.

Notes

The authors declare no competing financial interest.

■ REFERENCES

(1) Baker, M. B. Cloud Microphysics and Climate. *Science* **1997**, *276* (5315), 1072−1078.

(2) Baker, M. B.; Peter, T. Small-scale cloud processes and climate. *Nature* **2008**, *451* (7176), 299−300.

(3) Lohmann, U.; Feichter, J. Global indirect aerosol effects: a review. *Atmos. Chem. Phys.* **2005**, *5* (3), 715−737.

(4) Rosenfeld, D.; Sherwood, S.; Wood, R.; Donner, L. Climate Effects of Aerosol-Cloud Interactions. *Science* **2014**, *343* (6169), 379−380.

(5) Storelvmo, T. Aerosol Effects on Climate via Mixed-Phase and Ice Clouds. *Annu. Rev. Earth Planet. Sci.* **2017**, *45* (1), 199−222.

(6) Matus, A. V.; L'Ecuyer, T. S. The role of cloud phase in Earth's radiation budget. *J. Geophys. Res.: Atmos.* **2017**, *122* (5), 2559−2578.

(7) Mülmenstädt, J.; Sourdeval, O.; Delanoë, J.; Quaas, J. Frequency of occurrence of rain from liquid-mixed-and ice-phase clouds derived from A-Train satellite retrievals. *Geophys. Res. Lett.* **2015**, *42* (15), 6502−6509.

(8) Abbatt, J. P. D. Interactions of Atmospheric Trace Gases with Ice Surfaces: Adsorption and Reaction. *Chem. Rev.* **2003**, *103* (12), 4783−4800.

(9) Wang, P.-H.; Minnis, P.; McCormick, M. P.; Kent, G. S.; Skeens, K. M. A 6-year climatology of cloud occurrence frequency from Stratospheric Aerosol and Gas Experiment II observations (1985−1990). *J. Geophys. Res.* **1996**, *101*, 29,407−29,429.

(10) Held, I. M.; Soden, B. J. Water Vapor Feedback and Global Warming. *Annu. Rev. Energy Environ.* **2000**, *25* (1), 441−475.

(11) Lohmann, U.; Roeckner, E.; Collins, W. D.; Heymsfield, A. J.; McFarquhar, G. M.; Barnett, T. P. The role of water vapor and convection during the Central Equatorial Pacific Experiment from observations and model simulations. *J. Geophys. Res.: Atmos.* **1995**, *100* (D12), 26229−26245.

(12) Korolev, A.; McFarquhar, G.; Field, P. R.; Franklin, C.; Lawson, P.; Wang, Z.; Williams, E.; Abel, S. J.; Axisa, D.; Borrmann, S.; Crosier, J.; Fugal, J.; Krämer, M.; Lohmann, U.; Schlenczek, O.; Schnaiter, M.; Wendisch, M. Mixed-Phase Clouds: Progress and Challenges. *Meteorol. Monogr.* **2017**, *58*, 5.1−5.50.

(13) Korolev, A. Limitations of the Wegener-Bergeron-Findeisen Mechanism in the Evolution of Mixed-Phase Clouds. *J. Atmos. Sci.* **2007**, *64* (9), 3372−3375.

(14) Morrison, H.; de Boer, G.; Feingold, G.; Harrington, J.; Shupe, M. D.; Sulia, K. Resilience of persistent Arctic mixed-phase clouds. *Nat. Geosci.* **2012**, *5* (1), 11−17.

(15) Pruppacher, H.; Klett, J.; Wang, P. Microphysics of Clouds and Precipitation. *Aerosol Sci. Technol.* **1998**, *28*, 381−382.

(16) Kanji, Z. A.; Ladino, L. A.; Wex, H.; Boose, Y.; Burkert-Kohn, M.; Cziczo, D. J.; Krämer, M. Overview of Ice Nucleating Particles. *Meteorol. Monogr.* **2017**, *58*, 1.1−1.33.

(17) Burrows, S. M.; McCluskey, C. S.; Cornwell, G.; Steinke, I.; Zhang, K.; Zhao, B.; Zawadowicz, M.; Raman, A.; Kulkarni, G.; China, S.; Zelenyuk, A.; DeMott, P. J. Ice-Nucleating Particles That Impact Clouds and Climate: Observational and Modeling Research Needs. *Rev. Geophys.* **2022**, *60* (2), No. e2021RG000745.

(18) Möhler, O.; Stetzer, O.; Schaefers, S.; Linke, C.; Schnaiter, M.; Tiede, R.; Saathoff, H.; Krämer, M.; Mangold, A.; Budz, P.; Zink, P.; Schreiner, J.; Mauersberger, K.; Haag, W.; Kärcher, B.; Schurath, U. Experimental investigation of homogeneous freezing of sulphuric acid

particles in the aerosol chamber AIDA. *Atmos. Chem. Phys.* **2003**, *3* (1), 211−223.
(19) Heymsfield, A. J.; Miloshevich, L. M. Homogeneous Ice Nucleation and Supercooled Liquid Water in Orographic Wave Clouds. *J. Atmos. Sci.* **1993**, *50* (15), 2335−2353.
(20) Heymsfield, A. J.; Sabin, R. M. Cirrus Crystal Nucleation by Homogeneous Freezing of Solution Droplets. *J. Atmos. Sci.* **1989**, *46* (14), 2252−2264.
(21) Kärcher, B.; DeMott, P. J.; Jensen, E. J.; Harrington, J. Y. Studies on the Competition Between Homogeneous and Heterogeneous Ice Nucleation in Cirrus Formation. *J. Geophys. Res.: Atmos.* **2022**, *127* (3), No. e2021JD035805.
(22) Kärcher, B.; Lohmann, U. A parameterization of cirrus cloud formation: Heterogeneous freezing. *J. Geophys. Res.: Atmos.* **2003**, *108* (D14), 4402.
(23) Hoose, C.; Möhler, O. Heterogeneous ice nucleation on atmospheric aerosols: a review of results from laboratory experiments. *Atmos. Chem. Phys.* **2012**, *12* (20), 9817−9854.
(24) Ladino Moreno, L. A.; Stetzer, O.; Lohmann, U. Contact freezing: a review of experimental studies. *Atmos. Chem. Phys.* **2013**, *13* (19), 9745−9769.
(25) Murray, B. J.; Wilson, T. W.; Dobbie, S.; Cui, Z.; Al-Jumur, S. M. R. K.; Möhler, O.; Schnaiter, M.; Wagner, R.; Benz, S.; Niemand, M.; Saathoff, H.; Ebert, V.; Wagner, S.; Kärcher, B. Heterogeneous nucleation of ice particles on glassy aerosols under cirrus conditions. *Nat. Geosci.* **2010**, *3* (4), 233−237.
(26) Engelstaedter, S.; Tegen, I.; Washington, R. North African dust emissions and transport. *Earth-Sci. Rev.* **2006**, *79* (1−2), 73−100.
(27) Alpert, P. A.; Aller, J. Y.; Knopf, D. A. Ice nucleation from aqueous NaCl droplets with and without marine diatoms. *Atmos. Chem. Phys.* **2011**, *11* (12), 5539−5555.
(28) Augustin, S.; Wex, H.; Niedermeier, D.; Pummer, B.; Grothe, H.; Hartmann, S.; Tomsche, L.; Clauss, T.; Voigtländer, J.; Ignatius, K.; Stratmann, F. Immersion freezing of birch pollen washing water. *Atmos. Chem. Phys.* **2013**, *13* (21), 10989−11003.
(29) Hiranuma, N.; Hoffmann, N.; Kiselev, A.; Dreyer, A.; Zhang, K.; Kulkarni, G.; Koop, T.; Möhler, O. Influence of surface morphology on the immersion mode ice nucleation efficiency of hematite particles. *Atmos. Chem. Phys.* **2014**, *14* (5), 2315−2324.
(30) Huffman, J. A.; Prenni, A. J.; DeMott, P. J.; Pöhlker, C.; Mason, R. H.; Robinson, N. H.; Fröhlich-Nowoisky, J.; Tobo, Y.; Després, V. R.; Garcia, E.; Gochis, D. J.; Harris, E.; Müller-Germann, I.; Ruzene, C.; Schmer, B.; Sinha, B.; Day, D. A.; Andreae, M. O.; Jimenez, J. L.; Gallagher, M.; Kreidenweis, S. M.; Bertram, A. K.; Pöschl, U. High concentrations of biological aerosol particles and ice nuclei during and after rain. *Atmos. Chem. Phys.* **2013**, *13* (13), 6151−6164.
(31) Knopf, D. A.; Alpert, P. A.; Wang, B.; Aller, J. Y. Stimulation of ice nucleation by marine diatoms. *Nat. Geosci.* **2011**, *4* (2), 88−90.
(32) Mason, R. H.; Si, M.; Li, J.; Chou, C.; Dickie, R.; Toom-Sauntry, D.; Pöhlker, C.; Yakobi-Hancock, J. D.; Ladino, L. A.; Jones, K.; Leaitch, W. R.; Schiller, C. L.; Abbatt, J. P. D.; Huffman, J. A.; Bertram, A. K. Ice nucleating particles at a coastal marine boundary layer site: correlations with aerosol type and meteorological conditions. *Atmos. Chem. Phys.* **2015**, *15* (21), 12547−12566.
(33) Pandey, R.; Usui, K.; Livingstone, R. A.; Fischer, S. A.; Pfaendtner, J.; Backus, E. H. G.; Nagata, Y.; Fröhlich-Nowoisky, J.; Schmüser, L.; Mauri, S.; Scheel, J. F.; Knopf, D. A.; Pöschl, U.; Bonn, M.; Weidner, T. Ice-nucleating bacteria control the order and dynamics of interfacial water. *Sci. Adv.* **2016**, *2* (4), No. e1501630.
(34) Matthews, B. H.; Alsante, A. N.; Brooks, S. D. Pollen Emissions of Subpollen Particles and Ice Nucleating Particles. *ACS Earth Space Chem.* **2023**, *7* (6), 1207−1218.
(35) Cornwell, G. C.; McCluskey, C. S.; Hill, T. C. J.; Levin, E. T.; Rothfuss, N. E.; Tai, S.-L.; Petters, M. D.; DeMott, P. J.; Kreidenweis, S.; Prather, K. A.; Burrows, S. M. Bioaerosols are the dominant source of warm-temperature immersion-mode INPs and drive uncertainties in INP predictability. *Sci. Adv.* **2023**, *9* (37), No. eadg3715.
(36) Alpert, P. A.; Kilthau, W. P.; O'Brien, R. E.; Moffet, R. C.; Gilles, M. K.; Wang, B.; Laskin, A.; Aller, J. Y.; Knopf, D. A. Ice-nucleating agents in sea spray aerosol identified and quantified with a holistic multimodal freezing model. *Sci. Adv.* **2022**, *8* (44), No. eabq6842.
(37) Koop, T.; Ng, H. P.; Molina, L. T.; Molina, M. J. A New Optical Technique to Study Aerosol Phase Transitions: The Nucleation of Ice from H2SO4 Aerosols. *J. Phys. Chem. A* **1998**, *102* (45), 8924−8931.
(38) Knopf, D. A.; Lopez, M. D. Homogeneous ice freezing temperatures and ice nucleation rates of aqueous ammonium sulfate and aqueous levoglucosan particles for relevant atmospheric conditions. *Phys. Chem. Chem. Phys.* **2009**, *11* (36), 8056−8068.
(39) Koop, T.; Bertram, A. K.; Molina, L. T.; Molina, M. J. Phase Transitions in Aqueous NH4HSO4 Solutions. *J. Phys. Chem. A* **1999**, *103* (45), 9042−9048.
(40) Bertram, A. K.; Koop, T.; Molina, L. T.; Molina, M. J. Ice Formation in (NH4)2SO4-H2O Particles. *J. Phys. Chem. A* **2000**, *104* (3), 584−588.
(41) Knopf, D. A.; Alpert, P. A. Atmospheric ice nucleation. *Nat. Rev. Phys.* **2023**, *5* (4), 203−217.
(42) Hallquist, M.; Wenger, J. C.; Baltensperger, U.; Rudich, Y.; Simpson, D.; Claeys, M.; Dommen, J.; Donahue, N. M.; George, C.; Goldstein, A. H.; Hamilton, J. F.; Herrmann, H.; Hoffmann, T.; Iinuma, Y.; Jang, M.; Jenkin, M. E.; Jimenez, J. L.; Kiendler-Scharr, A.; Maenhaut, W.; McFiggans, G.; Mentel, T. F.; Monod, A.; Prévôt, A. S. H.; Seinfeld, J. H.; Surratt, J. D.; Szmigielski, R.; Wildt, J. The formation, properties and impact of secondary organic aerosol: current and emerging issues. *Atmos. Chem. Phys.* **2009**, *9* (14), 5155−5236.
(43) Jimenez, J. L.; Canagaratna, M. R.; Donahue, N. M.; Prevot, A. S. H.; Zhang, Q.; Kroll, J. H.; DeCarlo, P. F.; Allan, J. D.; Coe, H.; Ng, N. L.; Aiken, A. C.; Docherty, K. S.; Ulbrich, I. M.; Grieshop, A. P.; Robinson, A. L.; Duplissy, J.; Smith, J. D.; Wilson, K. R.; Lanz, V. A.; Hueglin, C.; Sun, Y. L.; Tian, J.; Laaksonen, A.; Raatikainen, T.; Rautiainen, J.; Vaattovaara, P.; Ehn, M.; Kulmala, M.; Tomlinson, J. M.; Collins, D. R.; Cubison, M. J.; Dunlea, J.; Huffman, J. A.; Onasch, T. B.; Alfarra, M. R.; Williams, P. I.; Bower, K.; Kondo, Y.; Schneider, J.; Drewnick, F.; Borrmann, S.; Weimer, S.; Demerjian, K.; Salcedo, D.; Cottrell, L.; Griffin, R.; Takami, A.; Miyoshi, T.; Hatakeyama, S.; Shimono, A.; Sun, J. Y.; Zhang, Y. M.; Dzepina, K.; Kimmel, J. R.; Sueper, D.; Jayne, J. T.; Herndon, S. C.; Trimborn, A. M.; Williams, L. R.; Wood, E. C.; Middlebrook, A. M.; Kolb, C. E.; Baltensperger, U.; Worsnop, D. R.; Worsnop, D. R. Evolution of Organic Aerosols in the Atmosphere. *Science* **2009**, *326* (5959), 1525−1529.
(44) Shrivastava, M.; Cappa, C. D.; Fan, J.; Goldstein, A. H.; Guenther, A. B.; Jimenez, J. L.; Kuang, C.; Laskin, A.; Martin, S. T.; Ng, N. L.; Petaja, T.; Pierce, J. R.; Rasch, P. J.; Roldin, P.; Seinfeld, J. H.; Shilling, J.; Smith, J. N.; Thornton, J. A.; Volkamer, R.; Wang, J.; Worsnop, D. R.; Zaveri, R. A.; Zelenyuk, A.; Zhang, Q. Recent advances in understanding secondary organic aerosol: Implications for global climate forcing. *Rev. Geophys.* **2017**, *55* (2), 509−559.
(45) Murphy, D. M.; Cziczo, D. J.; Froyd, K. D.; Hudson, P. K.; Matthew, B. M.; Middlebrook, A. M.; Peltier, R. E.; Sullivan, A.; Thomson, D. S.; Weber, R. J. Single-particle mass spectrometry of tropospheric aerosol particles. *J. Geophys. Res.: Atmos.* **2006**, *111* (D23), D23S32.
(46) Zhang, Q.; Jimenez, J. L.; Canagaratna, M. R.; Allan, J. D.; Coe, H.; Ulbrich, I.; Alfarra, M. R.; Takami, A.; Middlebrook, A. M.; Sun, Y. L.; Dzepina, K.; Dunlea, E.; Docherty, K.; DeCarlo, P. F.; Salcedo, D.; Onasch, T.; Jayne, J. T.; Miyoshi, T.; Shimono, A.; Hatakeyama, S.; Takegawa, N.; Kondo, Y.; Schneider, J.; Drewnick, F.; Borrmann, S.; Weimer, S.; Demerjian, K.; Williams, P.; Bower, K.; Bahreini, R.; Cottrell, L.; Griffin, R. J.; Rautiainen, J.; Sun, J. Y.; Zhang, Y. M.; Worsnop, D. R. Ubiquity and dominance of oxygenated species in organic aerosols in anthropogenically-influenced Northern Hemisphere midlatitudes. *Geophys. Res. Lett.* **2007**, *34* (13), L13801.
(47) Kanakidou, M.; Seinfeld, J. H.; Pandis, S. N.; Barnes, I.; Dentener, F. J.; Facchini, M. C.; Van Dingenen, R.; Ervens, B.; Nenes, A.; Nielsen, C. J.; Swietlicki, E.; Putaud, J. P.; Balkanski, Y.; Fuzzi, S.; Horth, J.; Moortgat, G. K.; Winterhalter, R.; Myhre, C. E. L.;

Tsigaridis, K.; Vignati, E.; Stephanou, E. G.; Wilson, J. Organic aerosol and global climate modelling: a review. *Atmos. Chem. Phys.* **2005**, *5* (4), 1053−1123.
(48) Froyd, K. D.; Murphy, D. M.; Sanford, T. J.; Thomson, D. S.; Wilson, J. C.; Pfister, L.; Lait, L. Aerosol composition of the tropical upper troposphere. *Atmos. Chem. Phys.* **2009**, *9* (13), 4363−4385.
(49) Schill, G. P.; Tolbert, M. A. Heterogeneous ice nucleation on phase-separated organic-sulfate particles: effect of liquid vs. glassy coatings. *Atmos. Chem. Phys.* **2013**, *13* (9), 4681−4695.
(50) Zobrist, B.; Marcolli, C.; Koop, T.; Luo, B. P.; Murphy, D. M.; Lohmann, U.; Zardini, A. A.; Krieger, U. K.; Corti, T.; Cziczo, D. J.; Fueglistaler, S.; Hudson, P. K.; Thomson, D. S.; Peter, T. Oxalic acid as a heterogeneous ice nucleus in the upper troposphere and its indirect aerosol effect. *Atmos. Chem. Phys.* **2006**, *6* (10), 3115−3129.
(51) Wagner, R.; Höhler, K.; Möhler, O.; Saathoff, H.; Schnaiter, M. Crystallization and immersion freezing ability of oxalic and succinic acid in multicomponent aqueous organic aerosol particles. *Geophys. Res. Lett.* **2015**, *42* (7), 2464−2472.
(52) Wagner, R.; Möhler, O.; H, S.; Schnaiter, M.; Leisner, T. New cloud chamber experiments on the heterogeneous ice nucleation ability of oxalic acid in the immersion mode. *Atmos. Chem. Phys. Discuss.* **2010**, *11*, 2083.
(53) Shilling, J. E.; Fortin, T. J.; Tolbert, M. A. Depositional ice nucleation on crystalline organic and inorganic solids. *J. Geophys. Res.: Atmos.* **2006**, *111* (D12), D12204.
(54) Baustian, K. J.; Wise, M. E.; Tolbert, M. A. Depositional ice nucleation on solid ammonium sulfate and glutaric acid particles. *Atmos. Chem. Phys.* **2010**, *10* (5), 2307−2317.
(55) Wagner, R.; Benz, S.; Möhler, O.; Saathoff, H.; Schnaiter, M.; Leisner, T. Influence of Particle Aspect Ratio on the Midinfrared Extinction Spectra of Wavelength-Sized Ice Crystals. *J. Phys. Chem. A* **2007**, *111* (50), 13003−13022.
(56) Prenni, A. J.; Petters, M. D.; Faulhaber, A.; Carrico, C. M.; Ziemann, P. J.; Kreidenweis, S. M.; DeMott, P. J. Heterogeneous ice nucleation measurements of secondary organic aerosol generated from ozonolysis of alkenes. *Geophys. Res. Lett.* **2009**, *36* (6), L06808.
(57) Möhler, O.; Benz, S.; Saathoff, H.; Schnaiter, M.; Wagner, R.; Schneider, J.; Walter, S.; Ebert, V.; Wagner, S. The effect of organic coating on the heterogeneous ice nucleation efficiency of mineral dust aerosols. *Environ. Res. Lett.* **2008**, *3* (2), 025007.
(58) Wang, B.; Lambe, A. T.; Massoli, P.; Onasch, T. B.; Davidovits, P.; Worsnop, D. R.; Knopf, D. A. The deposition ice nucleation and immersion freezing potential of amorphous secondary organic aerosol: Pathways for ice and mixed-phase cloud formation. *J. Geophys. Res.: Atmos.* **2012**, *117* (D16), D16209.
(59) Schill, G. P.; De Haan, D. O.; Tolbert, M. A. Heterogeneous Ice Nucleation on Simulated Secondary Organic Aerosol. *Environ. Sci. Technol.* **2014**, *48* (3), 1675−1682.
(60) Wolf, M. J.; Zhang, Y.; Zawadowicz, M. A.; Goodell, M.; Froyd, K.; Freney, E.; Sellegri, K.; Rösch, M.; Cui, T.; Winter, M.; Lacher, L.; Axisa, D.; DeMott, P. J.; Levin, E. J. T.; Gute, E.; Abbatt, J.; Koss, A.; Kroll, J. H.; Surratt, J. D.; Cziczo, D. J. A biogenic secondary organic aerosol source of cirrus ice nucleating particles. *Nat. Commun.* **2020**, *11* (1), 4834.
(61) Ladino, L. A.; Zhou, S.; Yakobi-Hancock, J. D.; Aljawhary, D.; Abbatt, J. P. D. Factors controlling the ice nucleating abilities of α-pinene SOA particles. *J. Geophys. Res.: Atmos.* **2014**, *119* (14), 9041−9051.
(62) Ignatius, K.; Kristensen, T. B.; Järvinen, E.; Nichman, L.; Fuchs, C.; Gordon, H.; Herenz, P.; Hoyle, C. R.; Duplissy, J.; Garimella, S.; Dias, A.; Frege, C.; Höppel, N.; Tröstl, J.; Wagner, R.; Yan, C.; Amorim, A.; Baltensperger, U.; Curtius, J.; Donahue, N. M.; Gallagher, M. W.; Kirkby, J.; Kulmala, M.; Möhler, O.; Saathoff, H.; Schnaiter, M.; Tomé, A.; Virtanen, A.; Worsnop, D.; Stratmann, F. Heterogeneous ice nucleation of viscous secondary organic aerosol produced from ozonolysis of <i>α</i>-pinene. *Atmos. Chem. Phys.* **2016**, *16* (10), 6495−6509.
(63) Piedehierro, A. A.; Welti, A.; Buchholz, A.; Korhonen, K.; Pullinen, I.; Summanen, I.; Virtanen, A.; Laaksonen, A. Ice nucleation on surrogates of boreal forest SOA particles: effect of water content and oxidative age. *Atmos. Chem. Phys.* **2021**, *21* (14), 11069−11078.
(64) Wagner, R.; Höhler, K.; Huang, W.; Kiselev, A.; Möhler, O.; Mohr, C.; Pajunoja, A.; Saathoff, H.; Schiebel, T.; Shen, X.; Virtanen, A. Heterogeneous ice nucleation of α-pinene SOA particles before and after ice cloud processing. *J. Geophys. Res.: Atmos.* **2017**, *122* (9), 4924−4943.
(65) Saukko, E.; Lambe, A. T.; Massoli, P.; Koop, T.; Wright, J. P.; Croasdale, D. R.; Pedernera, D. A.; Onasch, T. B.; Laaksonen, A.; Davidovits, P.; Worsnop, D. R.; Virtanen, A. Humidity-dependent phase state of SOA particles from biogenic and anthropogenic precursors. *Atmos. Chem. Phys.* **2012**, *12* (16), 7517−7529.
(66) Collier, K. N.; Brooks, S. D. Role of Organic Hydrocarbons in Atmospheric Ice Formation via Contact Freezing. *J. Phys. Chem. A* **2016**, *120* (51), 10169−10180.
(67) Berkemeier, T.; Shiraiwa, M.; Pöschl, U.; Koop, T. Competition between water uptake and ice nucleation by glassy organic aerosol particles. *Atmos. Chem. Phys.* **2014**, *14* (22), 12513−12531.
(68) Lei, Z.; Chen, Y.; Zhang, Y.; Cooke, M. E.; Ledsky, I. R.; Armstrong, N. C.; Olson, N. E.; Zhang, Z.; Gold, A.; Surratt, J. D.; Ault, A. P. Initial pH Governs Secondary Organic Aerosol Phase State and Morphology after Uptake of Isoprene Epoxydiols (IEPOX). *Environ. Sci. Technol.* **2022**, *56* (15), 10596−10607.
(69) Jang, M.; Czoschke, N. M.; Lee, S.; Kamens, R. M. Heterogeneous Atmospheric Aerosol Production by Acid-Catalyzed Particle-Phase Reactions. *Science* **2002**, *298* (5594), 814−817.
(70) Lin, Y.-H.; Zhang, Z.; Docherty, K. S.; Zhang, H.; Budisulistiorini, S. H.; Rubitschun, C. L.; Shaw, S. L.; Knipping, E. M.; Edgerton, E. S.; Kleindienst, T. E.; Gold, A.; Surratt, J. D. Isoprene Epoxydiols as Precursors to Secondary Organic Aerosol Formation: Acid-Catalyzed Reactive Uptake Studies with Authentic Compounds. *Environ. Sci. Technol.* **2012**, *46* (1), 250−258.
(71) Gaston, C. J.; Riedel, T. P.; Zhang, Z.; Gold, A.; Surratt, J. D.; Thornton, J. A. Reactive Uptake of an Isoprene-Derived Epoxydiol to Submicron Aerosol Particles. *Environ. Sci. Technol.* **2014**, *48* (19), 11178−11186.
(72) Jang, M.; Carroll, B.; Chandramouli, B.; Kamens, R. M. Particle Growth by Acid-Catalyzed Heterogeneous Reactions of Organic Carbonyls on Preexisting Aerosols. *Environ. Sci. Technol.* **2003**, *37* (17), 3828−3837.
(73) Prenni, A. J.; DeMott, P. J.; Kreidenweis, S. M. Water uptake of internally mixed particles containing ammonium sulfate and dicarboxylic acids. *Atmos. Environ.* **2003**, *37* (30), 4243−4251.
(74) Ghorai, S.; Laskin, A.; Tivanski, A. V. Spectroscopic Evidence of Keto-Enol Tautomerism in Deliquesced Malonic Acid Particles. *J. Phys. Chem. A* **2011**, *115* (17), 4373−4380.
(75) Rindelaub, J. D.; McAvey, K. M.; Shepson, P. B. The photochemical production of organic nitrates from α-pinene and loss via acid-dependent particle phase hydrolysis. *Atmos. Environ.* **2015**, *100*, 193−201.
(76) Ault, A. P.; Gaston, C. J.; Wang, Y.; Dominguez, G.; Thiemens, M. H.; Prather, K. A. Characterization of the Single Particle Mixing State of Individual Ship Plume Events Measured at the Port of Los Angeles. *Environ. Sci. Technol.* **2010**, *44* (6), 1954−1961.
(77) Longo, A. F.; Feng, Y.; Lai, B.; Landing, W. M.; Shelley, R. U.; Nenes, A.; Mihalopoulos, N.; Violaki, K.; Ingall, E. D. Influence of Atmospheric Processes on the Solubility and Composition of Iron in Saharan Dust. *Environ. Sci. Technol.* **2016**, *50* (13), 6912−6920.
(78) Fang, T.; Guo, H.; Zeng, L.; Verma, V.; Nenes, A.; Weber, R. J. Highly Acidic Ambient Particles, Soluble Metals, and Oxidative Potential: A Link between Sulfate and Aerosol Toxicity. *Environ. Sci. Technol.* **2017**, *51* (5), 2611−2620.
(79) Rapf, R. J.; Dooley, M. R.; Kappes, K.; Perkins, R. J.; Vaida, V. pH Dependence of the Aqueous Photochemistry of α-Keto Acids. *J. Phys. Chem. A* **2017**, *121* (44), 8368−8379.
(80) Liu, M. J.; Wiegel, A. A.; Wilson, K. R.; Houle, F. A. Aerosol Fragmentation Driven by Coupling of Acid-Base and Free-Radical

Chemistry in the Heterogeneous Oxidation of Aqueous Citric Acid by OH Radicals. *J. Phys. Chem. A* **2017**, *121* (31), 5856−5870.
(81) Losey, D. J.; Parker, R. G.; Freedman, M. A. pH Dependence of Liquid-Liquid Phase Separation in Organic Aerosol. *J. Phys. Chem. Lett.* **2016**, *7* (19), 3861−3865.
(82) Losey, D. J.; Ott, E. J. E.; Freedman, M. A. Effects of High Acidity on Phase Transitions of an Organic Aerosol. *J. Phys. Chem. A* **2018**, *122* (15), 3819−3828.
(83) Ren, Y.; Bertram, A. K.; Patey, G. N. Influence of pH on Ice Nucleation by Kaolinite: Experiments and Molecular Simulations. *J. Phys. Chem. A* **2022**, *126* (49), 9227−9243.
(84) Ren, Y.; Soni, A.; Kumar, A.; Bertram, A. K.; Patey, G. N. Effects of pH on Ice Nucleation by the α-Alumina (0001) Surface. *J. Phys. Chem. C* **2022**, *126* (46), 19934−19946.
(85) Surratt, J. D.; Lewandowski, M.; Offenberg, J. H.; Jaoui, M.; Kleindienst, T. E.; Edney, E. O.; Seinfeld, J. H. Effect of Acidity on Secondary Organic Aerosol Formation from Isoprene. *Environ. Sci. Technol.* **2007**, *41* (15), 5363−5369.
(86) Zhang, Y.; Chen, Y.; Lei, Z.; Olson, N. E.; Riva, M.; Koss, A. R.; Zhang, Z.; Gold, A.; Jayne, J. T.; Worsnop, D. R.; Onasch, T. B.; Kroll, J. H.; Turpin, B. J.; Ault, A. P.; Surratt, J. D. Joint Impacts of Acidity and Viscosity on the Formation of Secondary Organic Aerosol from Isoprene Epoxydiols (IEPOX) in Phase Separated Particles. *ACS Earth Space Chem.* **2019**, *3* (12), 2646−2658.
(87) Fornea, A. P.; Brooks, S. D.; Dooley, J. B.; Saha, A. Heterogeneous freezing of ice on atmospheric aerosols containing ash, soot, and soil. *J. Geophys. Res.: Atmos.* **2009**, *114* (D13), D13201.
(88) Langham, E. J.; Mason, B. J.-N.; Bernal, J. D. The heterogeneous and homogeneous nucleation of supercooled water. *Proc. R. Soc. London, Ser. A* **1958**, *247* (1251), 493−504.
(89) Budke, C.; Koop, T. BINARY: an optical freezing array for assessing temperature and time dependence of heterogeneous ice nucleation. *Atmos. Meas. Tech.* **2015**, *8* (2), 689−703.
(90) Knopf, D.; Luo, B.; Krieger, U.; Koop, T. Thermodynamic Dissociation Constant of the Bisulfate Ion from Raman and Ion Interaction Modeling Studies of Aqueous Sulfuric Acid at Low Temperatures. *J. Phys. Chem. A* **2003**, *107*, 4322−4332.
(91) Dawson, B. S. W.; Irish, D. E.; Toogood, G. E. Vibrational spectral studies of solutions at elevated temperatures and pressures. 8. A Raman spectral study of ammonium hydrogen sulfate solutions and the HSO/sub 4//sup −/−SO/sub 4//sup 2 -/equilibrium. *J. Phys. Chem.* **1986**, *90*, 334.
(92) Tomikawa, K.; Kanno, H. Raman Study of Sulfuric Acid at Low Temperatures. *J. Phys. Chem. A* **1998**, *102* (30), 6082−6088.
(93) Craig, R. L.; Bondy, A. L.; Ault, A. P. Computer-controlled Raman microspectroscopy (CC-Raman): A method for the rapid characterization of individual atmospheric aerosol particles. *Aerosol Sci. Technol.* **2017**, *51* (9), 1099−1112.
(94) Ault, A. P.; Zhao, D.; Ebben, C. J.; Tauber, M. J.; Geiger, F. M.; Prather, K. A.; Grassian, V. H. Raman microspectroscopy and vibrational sum frequency generation spectroscopy as probes of the bulk and surface compositions of size-resolved sea spray aerosol particles. *Phys. Chem. Chem. Phys.* **2013**, *15* (17), 6206−6214.
(95) Venkateswarlu, P.; Bist, H. D.; Jain, Y. S. Laser excited Raman spectrum of ammonium sulfate single crystal. *J. Raman Spectrosc.* **1975**, *3* (2−3), 143−151.
(96) Vargas Jentzsch, P.; Kampe, B.; Ciobotă, V.; Rösch, P.; Popp, J. Inorganic salts in atmospheric particulate matter: Raman spectroscopy as an analytical tool. *Spectrochim. Acta, Part A* **2013**, *115*, 697−708.
(97) Brizuela, A. B.; Bichara Lc Fau-Romano, E.; Romano E Fau-Yurquina, A.; Yurquina A Fau-Locatelli, S.; Locatelli S Fau-Brandán, S. A.; Brandán, S. A. A complete characterization of the vibrational spectra of sucrose. *Carbohydr Res.* **2012**, *361*, 212.
(98) Mathlouthi, M.; Vinh Luu, D. Laser-raman spectra of d-glucose and sucrose in aqueous solution. *Carbohydr. Res.* **1980**, *81* (2), 203−212.
(99) Bondy, A. L.; Craig, R. L.; Zhang, Z.; Gold, A.; Surratt, J. D.; Ault, A. P. Isoprene-Derived Organosulfates: Vibrational Mode Analysis by Raman Spectroscopy, Acidity-Dependent Spectral Modes, and Observation in Individual Atmospheric Particles. *J. Phys. Chem. A* **2018**, *122* (1), 303−315.
(100) Doughty, D. C.; Hill, S. C. Raman spectra of atmospheric aerosol particles: Clusters and time-series for a 22.5 hr sampling period. *J. Quant. Spectrosc. Radiat. Transfer* **2020**, *248*, 106907.
(101) Olson, N. E.; Lei, Z.; Craig, R. L.; Zhang, Y.; Chen, Y.; Lambe, A. T.; Zhang, Z.; Gold, A.; Surratt, J. D.; Ault, A. P. Reactive Uptake of Isoprene Epoxydiols Increases the Viscosity of the Core of Phase-Separated Aerosol Particles. *ACS Earth Space Chem.* **2019**, *3* (8), 1402−1414.
(102) Bondy, A. L.; Kirpes, R. M.; Merzel, R. L.; Pratt, K. A.; Banaszak Holl, M. M.; Ault, A. P. Atomic Force Microscopy-Infrared Spectroscopy of Individual Atmospheric Aerosol Particles: Subdiffraction Limit Vibrational Spectroscopy and Morphological Analysis. *Anal. Chem.* **2017**, *89* (17), 8594−8598.
(103) Lei, Z.; Bliesner, S. E.; Mattson, C. N.; Cooke, M. E.; Olson, N. E.; Chibwe, K.; Albert, J. N. L.; Ault, A. P. Aerosol Acidity Sensing via Polymer Degradation. *Anal. Chem.* **2020**, *92* (9), 6502−6511.
(104) Kucinski, T. M.; Dawson, J. N.; Freedman, M. A. Size-Dependent Liquid-Liquid Phase Separation in Atmospherically Relevant Complex Systems. *J. Phys. Chem. Lett.* **2019**, *10*, 6915−6920.
(105) You, Y.; Bertram, A. K. Effects of molecular weight and temperature on liquid-liquid phase separation in particles containing organic species and inorganic salts. *Atmos. Chem. Phys.* **2015**, *15* (3), 1351−1365.
(106) Koop, T.; Luo, B.; Tsias, A.; Peter, T. Water activity as the determinant for homogeneous ice nucleation in aqueous solutions. *Nature* **2000**, *406* (6796), 611−614.
(107) Wexler, A. S.; Clegg, S. L. Atmospheric aerosol models for systems including the ions H+, NH4+, Na+, SO42-NO3-Cl-Br-and H2O. *J. Geophys. Res.: Atmos.* **2002**, *107* (D14), ACH 14.
(108) Song, M.; Marcolli, C.; Krieger, U.; Zuend, A.; Peter, T. Liquid-liquid phase separation and morphology of internally mixed dicarboxylic acids/ammonium sulfate/water particles. *Atmos. Chem. Phys.* **2012**, *12*, 2691−2712.
(109) Bertram, A. K.; Martin, S. T.; Hanna, S. J.; Smith, M. L.; Bodsworth, A.; Chen, Q.; Kuwata, M.; Liu, A.; You, Y.; Zorn, S. R. Predicting the relative humidities of liquid-liquid phase separation, efflorescence, and deliquescence of mixed particles of ammonium sulfate, organic material, and water using the organic-to-sulfate mass ratio of the particle and the oxygen-to-carbon elemental ratio of the organic component. *Atmos. Chem. Phys.* **2011**, *11* (21), 10995−11006.
(110) Sobanska, S.; Hwang, H.; Choël, M.; Jung, H.-J.; Eom, H.-J.; Kim, H.; Barbillat, J.; Ro, C.-U. Investigation of the Chemical Mixing State of Individual Asian Dust Particles by the Combined Use of Electron Probe X-ray Microanalysis and Raman Microspectrometry. *Anal. Chem.* **2012**, *84* (7), 3145−3154.
(111) Zhou, Q.; Pang, S.-F.; Wang, Y.; Ma, J.-B.; Zhang, Y.-H. Confocal Raman Studies of the Evolution of the Physical State of Mixed Phthalic Acid/Ammonium Sulfate Aerosol Droplets and the Effect of Substrates. *J. Phys. Chem. B* **2014**, *118* (23), 6198−6205.
(112) Hyttinen, N.; Elm, J.; Malila, J.; Calderón, S. M.; Prisle, N. L. Thermodynamic properties of isoprene- and monoterpene-derived organosulfates estimated with COSMOtherm. *Atmos. Chem. Phys.* **2020**, *20* (9), 5679−5696.
(113) Larkin, P. *Infrared and Raman Spectroscopy: Principles and Spectral interpretation/Peter Larkin*; Elsevier: Amsterdam, Boston, 2011; p 228.
(114) Wise, M. E.; Baustian, K. J.; Tolbert, M. A.; Tolbert, M. A. Internally mixed sulfate and organic particles as potential ice nuclei in the tropical tropopause region. *Proc. Natl. Acad. Sci. U.S.A.* **2010**, *107* (15), 6693−6698.

https://doi.org/10.1021/acsearthspacechem.3c00242
ACS Earth Space Chem. 2023, 7, 2562−2573